

Soliton motion induced along ferromagnetic skyrmion chains in chiral thin nanotacks

J. C. Bellizotti Souza¹, N. P. Vizarim^{1,2}, C. J. O. Reichhardt³, C. Reichhardt³, P. A. Venegas⁴

¹*POSMAT - Programa de Pós-Graduação em Ciência e Tecnologia de Materiais, Faculdade de Ciências, Universidade Estadual Paulista - UNESP, Bauru, SP, CP 473, 17033-360, Brazil*

²*Department of Physics, University of Antwerp, Groenenborgerlaan 171, B-2020 Antwerp, Belgium*

³*Theoretical Division and Center for Nonlinear Studies, Los Alamos National Laboratory, Los Alamos, New Mexico 87545, USA*

⁴*Departamento de Física, Faculdade de Ciências, Unesp-Universidade Estadual Paulista, CP 473, 17033-360 Bauru, SP, Brazil*

Abstract

Using atomistic magnetic simulations we investigate the soliton motion along a pinned skyrmion chain containing an interstitial skyrmion. We find that the soliton can exhibit stable motion along the chain without a skyrmion Hall effect for an extended range of drives. Under a constant drive the solitons have a constant velocity. We also measure the skyrmion velocity-current curves and identify the signatures of different phases including a pinned phase, stable soliton motion, and quasi-free motion at higher drives where all of the skyrmions depin from the pinning centers and move along the rigid wall. In the quasi-free motion regime, the velocity is oscillatory due to the motion of the skyrmions over the pinning sites. For increasing pinning strength, the onset of soliton motion shifts to higher values of current density. We also find that for stronger pinning, the characteristic velocity-current shape is affected by the annihilation of single or multiple skyrmions in the drive interval over which the soliton motion occurs. Our results indicate that stable skyrmion soliton motion is possible and could be useful for technological applications.

Keywords: Skyrmion, solitons, transport

1. Introduction

There is great interest in finding solid state methods that permit more rapid information transport. Recent studies along these lines involve the use of topologically stable objects as information carriers due to their stability, low dimensionality, and ability to be manipulated. Notable examples used in both the fundamental and applied research communities include quantum Hall states, chiral edge states of topological insulators, and massless Majorana modes. [1–3]. In the context of magnetism, topological objects such as solitons, vortices, and monopoles are promising information carrier candidates due to their low-dimensional characteristics. Notably, the recent experimental observations of magnetic skyrmions in chiral thin films or magnetic bulk crystals [4–6] have introduced a new class to the family of topological magnetic objects. Due to their reduced

size, easy current-driven motion, and topological stability, magnetic skyrmions are intensely studied for the development of new integrated circuits that can facilitate more reliable, compact, and energy-efficient information transport.

Magnetic skyrmions are topologically protected spin textures [7] that arise in magnetic materials and exhibit particle-like behavior under small driving forces [4, 5, 7, 8]. Due to their smaller size and reduced energy cost, skyrmions are promising candidates for spintronics devices [7, 9, 10], such as magnetic logic gates [11–13], transistors [14] and diodes [12, 15–21]. Many proposals for applications in spintronics devices require precise control of skyrmion motion [6, 11, 13, 22–24]. Skyrmions share similarities with other overdamped particles, such as superconducting vortices, colloids, and electrons on Wigner crystals. These particles minimize their mutual interaction energy by forming a triangular lattice, and they can be driven by external forces while interacting with pinning sites in the material [25]. A key distinction between skyrmions and other overdamped particles is the presence of a strong non-dissipative Magnus force. This force generates a velocity component perpendicular to the net forces acting on the skyrmion, and the sign of this velocity component depends on the topological charge of the skyrmion [7, 8, 26–30]. In clean samples, where there are no defects with which the skyrmions can interact, the skyrmion motion occurs along an angle θ_{sk}^{int} , known as the skyrmion intrinsic Hall angle [7, 8, 26–29], with respect to the externally applied driving force. Under specific conditions, the skyrmion Hall angle can be zero, depending on the phenomenological Gilbert damping parameter and non-adiabatic spin transfer torque [26, 31]. The skyrmion Hall angle also depends on parameters such as the skyrmion size, with experimental results showing skyrmion Hall angles up to 50° [8, 25, 27, 30, 32], but larger angles are also possible depending on material parameters [7, 25]. For many applications the skyrmion Hall angle can be a limiting factor since the skyrmions can travel to the edge of the sample and be annihilated there, so there is great interest in identifying ways to move skyrmions under conditions of zero skyrmion Hall angle.

To harness the potential of skyrmions for spintronic applications, precise control of both individual and collective skyrmion motion has been investigated intensively. Various methods have been explored, such as periodic pinning [33–41], ratchet effects [42–45], interface guided motion [46, 47], magnetic and temperature gradients [48–51], sample curvature [52–54], skyrmion-vortex coupling using a ferromagnetic-superconductor heterostructure [55], skyrmion lattice compression [56, 57], and laminar and turbulent flow of skyrmions [58]. In the case of skyrmions interacting with periodic substrates, commensurability effects are crucial for determining the dynamical behavior of the skyrmions. Commensurability occurs when the ratio of the number of skyrmions N_{sk} to the number of pinning centers N_p is an integer or rational fraction. The effects of commensurability have been extensively studied in systems such as superconducting vortices [59–61], colloidal particles [62], Wigner crystals [63] and vortices in Bose-Einstein condensates [64, 65], but exploration of commensurability in skyrmion systems has been limited despite the expectation that new phenomena will arise due to the Magnus force [66, 67]. When the system is close to but not at a commensurate state, most of the sample is ordered but there can be well defined incommensurations in the form of solitons (kinks) or antisolitons (antikinks) that act like quasiparticles with their own dynamics. There can be an extended range of external drives where the solitons are depinned while the commensurate background remains pinned. The sliding dynamics of solitons on periodic substrates has been studied for superconducting vortices [60, 68], colloids [69–71], and frictional systems [72].

In a recent proposal, solitons moving through skyrmion chains were used as information carriers rather than the skyrmions themselves, and this approach was explored using a particle-based model [73]. The skyrmions are stabilized in a sample with a periodic array of attractive defects, and by

adding or removing a skyrmion from one of the rows of the array, a vacancy or interstitial soliton can be created. Under an applied current, the soliton moves while most of the skyrmions remain pinned. The main advantage of this technique is that the soliton is stable and can be set into motion with very low applied transport currents that are even smaller than the currents needed to depin the bulk of the skyrmions. These findings pave the way for fast and energy-efficient information transport in potential skyrmion devices; however, some important details remain to be explored, since the limitations of the particle model leave certain questions unanswered. For example, it is not known if the soliton can be stabilized when the skyrmions are not rigid but have internal degrees of freedom, nor has the stability of the soliton been tested in a dynamic context where skyrmion creation and/or annihilation is possible. Answering these and other questions requires a more detailed microscopic analysis.

In this work we use atomistic magnetic simulations to investigate the dynamical behavior of a skyrmion chain slightly away from commensuration, where an extra skyrmion is stabilized as an interstitial. In order to confine the skyrmions and guide their motion, we introduce a rigid wall above and below the line of pinning centers. The interstitial skyrmion depins at lower driving forces than the other skyrmions, creating a soliton pulse that propagates through the sample. In our work we provide a detailed description of the soliton motion and analyze the different dynamical phases that occur when the external driving force is varied. By adjusting the pinning strength, we determine the conditions under which the soliton can exist as well as the annihilation conditions required to destroy the soliton motion. In particular, we discover a reentrant pinning phase that arises due to the annihilation of the interstitial skyrmion, which destroys the soliton motion and prevents further motion. These new findings are only possible through a microscopic approach. These results can be applied to the design of new skyrmionic devices in which more efficient transport of information is achieved.

2. Simulation

We consider a thin ferromagnetic nanotrack of size 544 nm \times 34 nm placed in the $x-y$ plane that can support Ne  l skyrmions at $T = 0$ K under the influence of a magnetic field applied perpendicular to the film surface, as illustrated in Fig. 1. The sample has periodic boundary conditions along the x direction. In this nanotrack, two rigid magnetic walls of thickness $\Delta y = 14$ nm are placed along $y = 0$ nm and $y = 34$ nm. Thus, the only place in which skyrmions are able to reside is between the walls in the red region where $m_z = 1$, as shown in Fig. 1. Embedded in the ferromagnetic nanotrack are $N_p = 32$ equally spaced attractive pinning centers. We investigate the dynamical behavior of a skyrmion chain that is slightly away from commensuration with $N_{sk} = 33$ skyrmions. Note that due to the mismatch $N_{sk}/N_p = 1.03$ between skyrmions and pinning centers, one skyrmion stabilizes in an interstitial position between pinning sites.

Our simulations are performed with the atomistic model [74] for simulating individual atomic magnetic moments. The Hamiltonian is [26, 75, 76]:

$$\begin{aligned} \mathcal{H} = & - \sum_{i,j \in N} J_{ij} \mathbf{m}_i \cdot \mathbf{m}_j - \sum_{i,j \in N} \mathbf{D}_{ij} \cdot (\mathbf{m}_i \times \mathbf{m}_j) - \sum_i \mu \mathbf{H} \cdot \mathbf{m}_i \\ & - \sum_{i \notin P} K_0 (\mathbf{m}_i \cdot \hat{\mathbf{z}})^2 - \sum_{i \in P} K (\mathbf{m}_i \cdot \hat{\mathbf{z}})^2 \end{aligned} \quad (1)$$

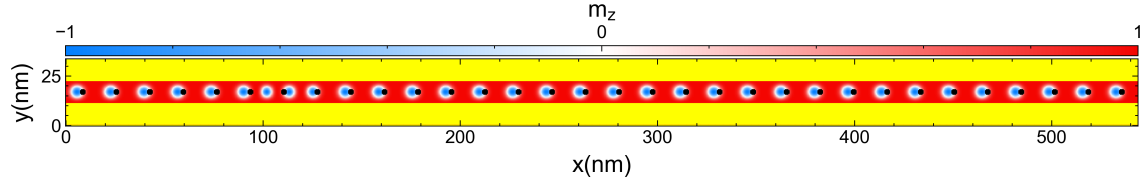


Figure 1: Image of the starting spin configuration for all simulations. Black dots are the pinning centers where the easy-plane anisotropy $K < 0$. Yellow represents rigid magnetic walls with $\mathbf{m} = \hat{\mathbf{z}}$. Skyrmions with $m_z = -1$ are able to exist in the red region, where the background magnetic field is $m_z = 1$. We consider conditions under which there is one skyrmion per pinning center along with one extra skyrmion located in the space between two pinning centers (shown at around $x = 100\text{nm}$), giving a ratio of $(32 + 1)/32 = 1.03$ skyrmions per pinning center.

The first term on the right hand side is the exchange interaction with N neighboring spins, and the second term is the Dzyaloshinskii–Moriya interaction for thin films. The third term is the Zeeman interaction with an applied magnetic field \mathbf{H} , where μ is the magnitude of the atomic magnetic moments. The last two terms are anisotropy interactions, with the fourth term representing the sample anisotropy and the fifth term the anisotropy produced by the set of P locations in which pinning centers reside. The pinning center anisotropy must be an easy-plane anisotropy in order to attract the skyrmion border. This is achieved by selecting K such that $K < 0$ [77]. The rigid walls confining the skyrmion chain are modeled as a fixed atomic magnetic moment with $\mathbf{m}_{\in W} = \hat{\mathbf{z}}$ where W is the set of locations composing the wall.

The time evolution of the system is described by the LLG equation augmented with the adiabatic spin-transfer torque: [26, 75, 76, 78, 79]:

$$\frac{d\mathbf{m}_i}{dt} = -\gamma\mathbf{m}_i \times \mathbf{H}_i^{\text{eff}} + \alpha\mathbf{m}_i \times \frac{d\mathbf{m}_i}{dt} + \frac{pa^3}{2e} (\mathbf{j} \cdot \nabla) \mathbf{m}_i \quad (2)$$

Here γ is the gyromagnetic ratio given by $\gamma = g\mu_B/\hbar$, α is the Gilbert damping parameter, $\mathbf{H}_i^{\text{eff}} = -\frac{1}{\mu} \frac{\partial \mathcal{H}}{\partial \mathbf{m}_i}$ is the effective magnetic field which encapsulates all interactions from the Hamiltonian, and the last term is the applied current where p is the polarization, e is the electron charge, a is the lattice constant, and \mathbf{j} is the applied current density. The model for the current includes the assumption that the conduction electron spins are parallel to the local magnetic moments \mathbf{m} [26, 80]. This type of current is called the spin-transfer torque, and its inclusion implies that the applied current is adiabatic. Non-adiabatic terms are not considered here since they do not affect the dynamical behavior of rigid nanoscale skyrmions at small driving forces [8], which is the regime we consider in this work. We apply the current in the $+y$ direction, $\mathbf{j} = j\hat{\mathbf{y}}$, based on previous works detailing interactions of skyrmions with magnetic walls [15, 16, 56].

The number of skyrmions in the sample is measured using topological charge calculations, and each skyrmion has $Q = \pm 1$ depending on the direction of the applied magnetic field [81]. The skyrmion velocities are calculated using the emergent electromagnetic fields [76]:

$$E_i^{\text{em}} = \frac{\hbar}{e} \mathbf{m} \cdot (\partial_t \mathbf{m} \times \partial_t \mathbf{m}) \quad B_i^{\text{em}} = \frac{\hbar}{2e} \varepsilon_{ijk} \mathbf{m} \cdot (\partial_j \mathbf{m} \times \partial_k \mathbf{m}) \quad (3)$$

where ε_{ijk} is the totally anti-symmetric tensor. The drift velocity of the skyrmions is then computed according to $\mathbf{E}^{\text{em}} = -\mathbf{v}_d \times \mathbf{B}^{\text{em}}$ [76, 82].

Throughout the simulation we fix $\alpha = 0.3$, $p = 1.0$ and $a = 0.5\text{nm}$. For the material parameters we choose $J = 1 \text{ meV}$, $D = 0.18J$ and $K_0 = 0.02J$. The applied field is $\mu\mathbf{H} = 0.5(D^2/J)\hat{\mathbf{z}}$,

corresponding to the skyrmion phase [26, 76]. This field creates skyrmions with $Q = -1$ topological charge.

In all simulations we start our system with a spin configuration, illustrated in Fig 1, obtained by inducing the formation of 33 skyrmions and then relaxing the LLG equation in Eq. 2 with $\mathbf{j} = 0$ for several time steps until reaching a steady configuration. After the sample has been initialized, we apply a spin current $\mathbf{j} \neq 0$ and begin measuring the dynamics of the system. We integrate Eq. 2 using a fourth order Runge-Kutta method. Simulation time units are normalized to $t = (\hbar/J)\tau$ and current density to $\mathbf{j} = (2eJ/a^2\hbar)\mathbf{j}'$. The values of time and current density reported here have been converted back into dimensional physical units.

3. Soliton Motion

We first consider the system shown in Fig. 1 using $K = -0.02J$ and $j = 2.04 \times 10^{10} \text{ A/m}^2$. In this case, the transport current is weak enough so that skyrmion annihilation never occurs. In Fig. 2 the skyrmion average velocity signals $\langle v_x \rangle$ and $\langle v_y \rangle$ are plotted as a function of time, t . Initially, for $t < 1$ ns, there is a transient motion while the skyrmions adjust themselves to the presence of the applied transport current combined with the rigid walls and pinning centers. Such transient motion occurs for low values of applied transport current and is crucial for establishing a dynamical stabilization that prevents skyrmion annihilation. For stronger currents, the transient stabilization process is more abrupt and annihilation may occur. Once $t > 1$ ns, the skyrmions always exhibit an average velocity $\langle v_x \rangle > 0$ indicating that collective skyrmion motion is occurring. For the range $1 < t < 2.5$ ns, the velocities are not completely periodic since the transient stabilization of the motion is not yet complete; however, for $t > 3$ ns, the skyrmion velocities exhibit a smooth periodic behavior as shown in the inset of Fig. 2. Note that while $\langle v_x \rangle$ oscillates around $\langle v_x \rangle \approx 1.25$ m/s, $\langle v_y \rangle$ oscillates around zero, meaning that there is a net motion along x but only bounded periodic excursions along y . The steady state $\langle v_x \rangle$ curve consists of repetitions of two peaks and one valley. This motion is associated with a soliton in the skyrmion chain, where the interstitial skyrmion pushes its neighboring pinned skyrmion out of a pinning center and takes up residence in the pinning center. The previously pinned skyrmion becomes the new interstitial.

In Fig. 3 we illustrate the soliton motion from one interstitial site to another using snapshots of a portion of the sample taken at consecutive values of t . At $t = 23.7$ ns in Fig. 3(a), the interstitial skyrmion causes a previously pinned skyrmion to depin due to the repulsive skyrmion-skyrmion interaction. In Fig. 3(b) at $t = 23.9$ ns, the interstitial skyrmion becomes pinned, and the previously pinned skyrmion becomes the new interstitial skyrmion. In Fig. 3(c) and (d) the same process described in Fig. 3(a) and (b) repeats for the next pair of skyrmions to the right, indicating the cascading process of depinning and pinning of skyrmions. The two peaks in $\langle v_x \rangle$ shown in the inset of Fig. 2 correspond to the depinning of a skyrmion from a pinning center (weaker peak) and the velocity boost caused by the interaction with the rigid wall above (stronger peak). The valley in $\langle v_x \rangle$ occurs when the moving interstitial skyrmion approaches its pinned neighbor skyrmion and slows down while pushing it until the pinned skyrmion begins to move. This process occurs as a repeating sequence, as demonstrated in Vizirim *et al.* using a particle-based model [73]. Here we show that this soliton motion remains robust even when using a more detailed micromagnetic model.

For the system illustrated in Figs. 2 and 3, it takes roughly 0.5 ns for the soliton to translate from one interstitial site to the next. The distance between pinning sites is 17 nm. Thus, the soliton velocity is $\langle v_s \rangle \approx 34$ m/s along the x direction. Comparing this value to the average

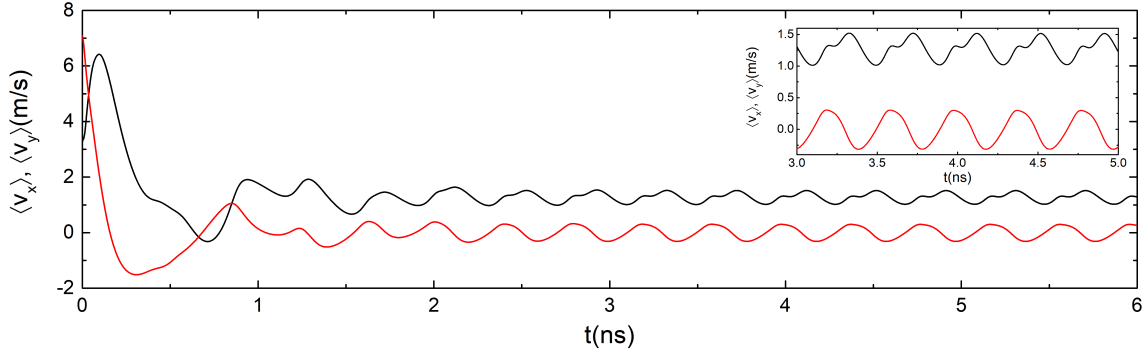


Figure 2: Skyrmion average velocity signals $\langle v_x \rangle$ (black) and $\langle v_y \rangle$ (red) for a system with $K = -0.02J$ and $j = 2.04 \times 10^{10} \text{ A/m}^2$. Here the plot is truncated after $t = 6$ ns, but the pattern established in both $\langle v_x \rangle$ and $\langle v_y \rangle$ repeats until the end of the simulation at $t = 59.2$ ns.

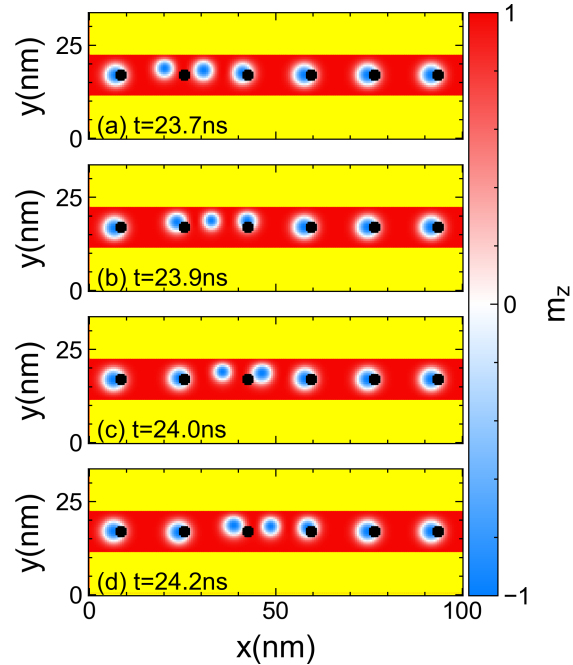


Figure 3: Snapshots of the spin configuration time evolution for a sample with $K = -0.02J$ and $j = 2.04 \times 10^{10} \text{ A/m}^2$. (a) $t = 23.7$ ns. (b) $t = 23.9$ ns. (c) $t = 24.0$ ns. (d) $t = 24.2$ ns. The soliton moves from its location between the second and third pinning sites from the left to a new location between the third and fourth pinning sites from the left. An animation of this motion is available in the supplementary material ‘‘mov-fig3.mp4’’.

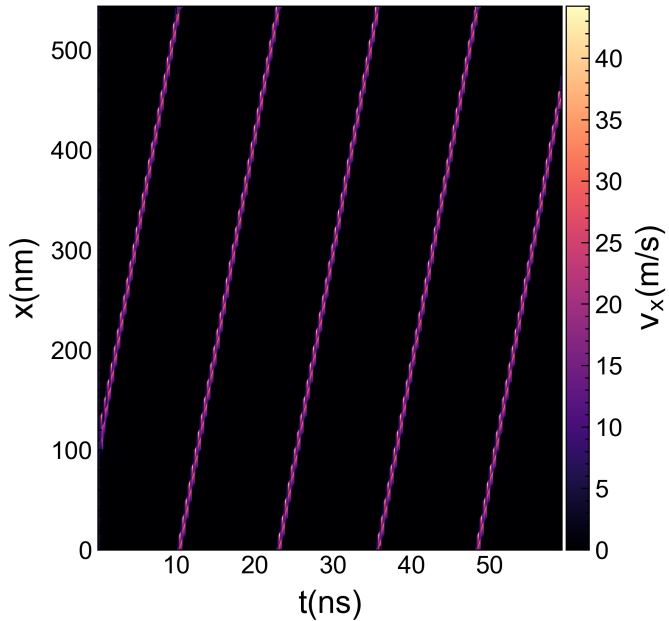


Figure 4: Heat map of skyrmion velocity v_x as a function of x versus time t for the system in Fig 3. Brighter colors represent faster skyrmions. The periodic discontinuities of the lines are produced when the skyrmion passes through the periodic boundary conditions in the x direction.

skyrmion velocity shown in Fig. 2, we find that the soliton moves much faster than the individual skyrmions. This indicates that the soliton could be employed as a very fast information carrier using low applied transport currents.

Fig 4 shows a heat map of the skyrmion velocity v_x plotted as a function of x position versus time t . This plot enables us to visualize the soliton motion through the sample and record its velocity. The periodic boundary conditions cause a discontinuity of the soliton motion each time the soliton exits the right side of the simulation box and reenters on the opposite side. As can be seen, all skyrmions except the ones supporting the soliton pulse are pinned and therefore have $v_x = 0$ m/s, whereas the skyrmions under the soliton have $v_x \neq 0$ m/s. The area of finite v_x indicates the trajectory of the perturbation over time. An interesting characteristic of the soliton motion is its linear behavior. As shown in Fig 4, the soliton perturbation moves across the sample with a constant velocity over time. It is also possible to estimate the soliton velocity from this plot since the soliton traverses the entire simulation box of 544 nm in roughly 14 ns, giving $\langle v_s \rangle \approx 38$ m/s.

4. Magnitude of Transport Current

In the last section we demonstrated that the soliton motion can be stabilized in the ferromagnetic nanotrack shown in Fig. 1 for a specific value of transport current. Now we investigate the stability of the soliton motion as the transport current is modified for fixed $K = -0.02J$. We vary the current density magnitude over the interval $2.9 \times 10^9 \text{ A/m}^2 \leq j \leq 5.8 \times 10^{10} \text{ A/m}^2$. Figure 5(a)

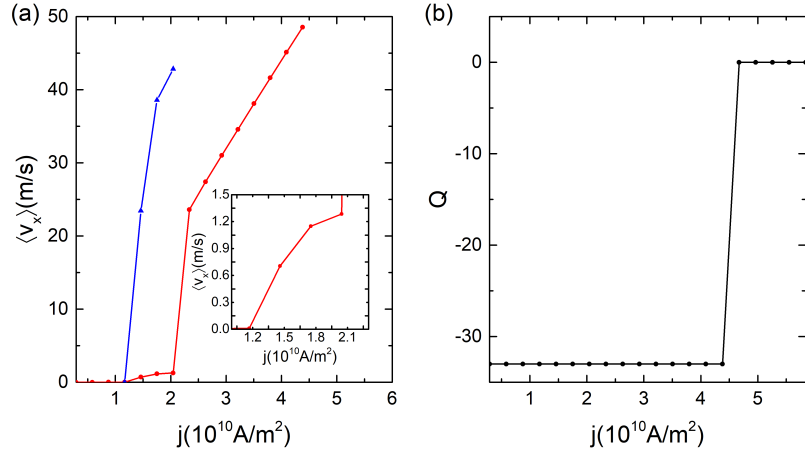


Figure 5: (a) The average velocity $\langle v_x \rangle$ vs applied transport density j for the skyrmions (red) and the soliton (blue). (b) The corresponding Q vs j . The inset of (a) shows a blowup of the average skyrmion velocity $\langle v_x \rangle$ vs j focusing on the soliton regime in the interval $1.1 \times 10^{10} \leq j \leq 2.3 \times 10^{10}$ A/m 2 . In (b) the topological charge changes from $Q = -33$ to $Q = 0$ in a sharp step around $j = 4.4 \times 10^{10}$ A/m 2 , well above the value of j for which all of the skyrmions have depinned.

shows the velocity signal $\langle v_x \rangle$ as a function of the applied transport current magnitude j . The inset in Fig 5(a) is a blowup of the main panel over the interval $1.1 \times 10^{10} \leq j \leq 2.3 \times 10^{10}$ A/m 2 . Three dynamic phases appear. For low currents of $j < 1.2 \times 10^{10}$ A/m 2 , there is a pinned phase where all of the skyrmions in the sample are pinned and the interstitial skyrmion remains trapped by the caging potential created by its neighboring pinned skyrmions. In the interval $1.2 \times 10^{10} \leq j \leq 2.1 \times 10^{10}$ A/m 2 , highlighted in the inset of Fig. 5(a), we find a soliton motion phase, where the soliton perturbation moves along the skyrmion chain at a high velocity. For the range $2.1 \times 10^{10} < j \leq 5.8 \times 10^{10}$ A/m 2 , we observe quasi-free skyrmion motion where all of the skyrmions depin and flow through the sample at increased velocity. Interestingly, the average soliton velocity increases monotonically with j until the soliton is destroyed, and the average soliton velocity is always higher than the average skyrmion velocity. The shape of the skyrmion velocity-current curve is consistent with previous work on soliton motion in skyrmion chains performed with a particle model [73]. Note that here, we use a microscopic model rather than a phenomenological model for the interaction between skyrmions and pinning centers. According to the pinning center potentials described in Ref. [77], pinning centers created using variations in anisotropy are attractive to skyrmions off-center, meaning that they attract the skyrmion domain wall but repel the skyrmion core. As a result, the skyrmions prefer to sit off-center in the pinning site. On the other hand, the phenomenological pinning centers used in Ref. [73] were modeled as parabolic traps that attract the skyrmion center, allowing the skyrmions to become pinned precisely at the center of pins. This small but significant difference in the skyrmion-pinning interaction may result in different behaviors.

In Fig. 5(b) we plot the stable topological charge Q , obtained after the initial transient annihilation process is complete, as a function of applied current density j . As can be seen in Fig. 1, there are 33 skyrmions in the sample, giving $Q = -33$. The value is negative due to the direction of the in-plane magnetization of the skyrmion core. Combining this information with the curve in Fig. 5(b), we can conclude that no skyrmions are annihilated for $j \leq 4.7 \times 10^{10}$ A/m 2 . Thus all three

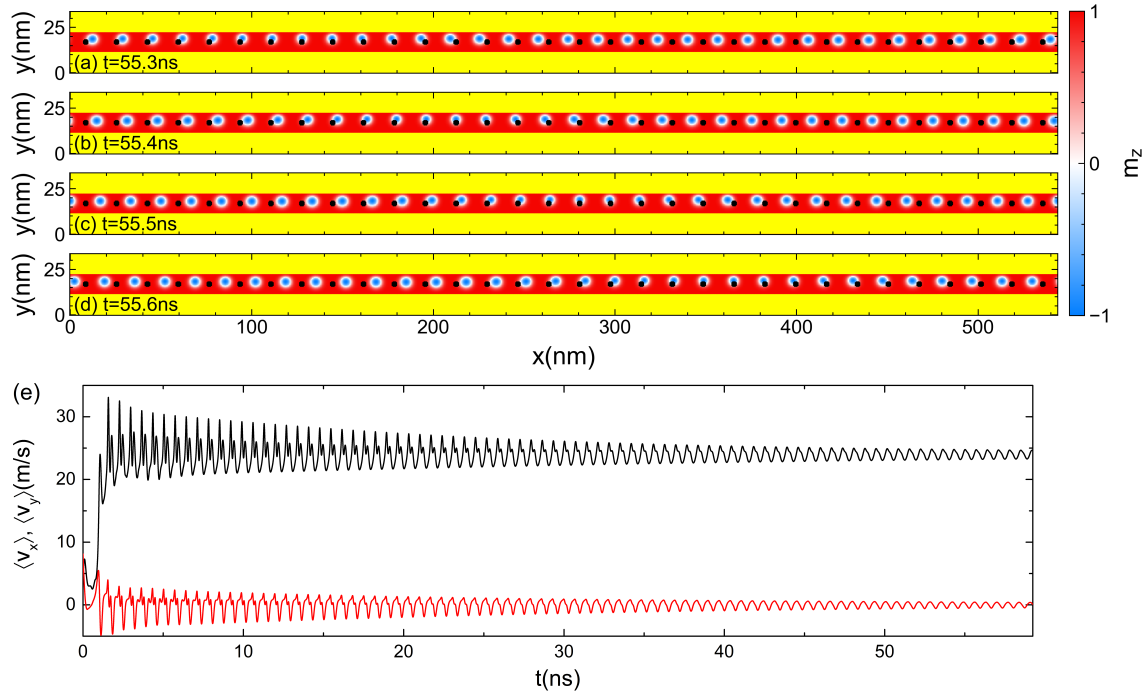


Figure 6: (a-d) Snapshots of the time evolution of the spin configuration for a system with $K = -0.02J$ and $j = 2.3 \times 10^{10} \text{ A/m}^2$, where all of the skyrmions have depinned from the pinning centers. (a) $t = 55.3$ ns. (b) $t = 55.4$ ns. (c) $t = 55.5$ ns. (d) $t = 55.6$ ns. An animation showing the complete time evolution is available in the Supplemental Material as “mov-fig6.mp4”. (e) Velocity signals $\langle v_x \rangle$ (black) and $\langle v_y \rangle$ (red) vs time t for the same system.

of the phases described above overlap with current density regions where the number of skyrmions is stable as a function of time. Once the annihilation process begins, however, it is irreversible since all of the skyrmions in the sample will annihilate if given sufficient time.

The interaction with pinning centers during the quasi-free skyrmion motion is illustrated in detail in Fig 6 for the system from Fig. 5 at $K = -0.02J$ and $j = 2.3 \times 10^{10} \text{ A/m}^2$. The time evolution of the spin configuration in Fig. 6(a-d) shows that the transport current is large enough to depin all of the skyrmions from the pinning centers at the same time. The skyrmions still feel the influence of the pinning sites, however, creating a perturbation that propagates through the skyrmion chain. A portion of the skyrmions are closer to the pinning sites and have reduced velocities. Meanwhile, other skyrmions are further from the pinning sites and flow faster. The combination of these two motions and the interchange of skyrmions between them creates a wave that propagates through the nanotrack. This motion has a much higher velocity than what we observe for the interstitial soliton. Fig. 6(e) shows the time dependent velocities $\langle v_x \rangle$ and $\langle v_y \rangle$ for this system. The initial motion is very chaotic and generates many peaks and valleys in $\langle v_x \rangle$ and $\langle v_y \rangle$. As time passes the system settles into periodic motion, and for $t > 45$ ns both $\langle v_x \rangle$ and $\langle v_y \rangle$ oscillate around stable values of $\langle v_x \rangle \approx 24$ m/s and $\langle v_y \rangle \approx 0$ m/s.

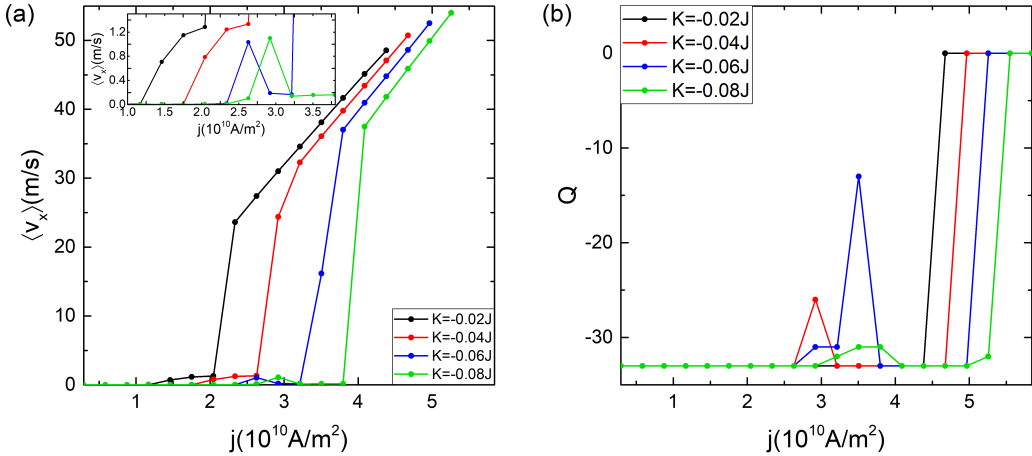


Figure 7: Plots of (a) $\langle v_x \rangle$ vs j and (b) Q vs j for four values of pinning strength, $K = -0.02J$ (black), $-0.04J$ (red), $-0.06J$ (blue), and $-0.08J$ (green). The inset of panel (a) shows a blow up of the soliton motion regime. As the pinning strength increases, the onset of soliton motion shifts to higher values of j . For very strong pinning, $|K| \geq 0.06J$, the soliton motion disappears and is replaced by a reentrant pinning phase due to skyrmion annihilation. The annihilation process is visible in panel (b) where, due to the annihilation of two skyrmions or one skyrmion for $K = -0.06J$ and $K = -0.08J$, the system becomes pinned again until stronger currents force all of the skyrmions to move. An animation showing the reentrant pinning phase is available in the Supplemental Material as “movfig7.mp4”.

5. Pinning Center Strength

In this section we investigate how the anisotropy strength of the pinning sites affects the dynamics. We choose values of K from the range $-0.08J \leq K \leq -0.02J$. For the easy-plane anisotropy we require $K < 0$, and larger values of $|K|$ enhance the easy-plane anisotropy. That is, larger values of $|K|$ produce a stronger attractive interaction between a skyrmion and a pinning site. Figure 7(a) shows the velocity $\langle v_x \rangle$ versus applied current density j for specific values of K . The inset of Fig. 7(a) shows a blow up of the soliton motion regime. As $|K|$ increases, the onset of soliton motion shifts to higher values of j . Such behavior is expected since stronger skyrmion-pinning interactions make it necessary to apply a higher transport current in order to depin the skyrmions. The depinning currents are $j_c = 1.2 \times 10^{10} \text{ A/m}^2$, $1.8 \times 10^{10} \text{ A/m}^2$, $2.3 \times 10^{10} \text{ A/m}^2$ and $2.6 \times 10^{10} \text{ A/m}^2$ for $K = -0.02J$, $-0.04J$, $-0.06J$ and $-0.08J$, respectively. Note that there is an intermediate point of increased $\langle v_x \rangle$ for the $K = -0.08J$ curve, visible in the inset of Fig. 7(a). This point does not indicate the existence of soliton motion. Instead, there is only a transient motion that ceases after 25 ns. As discussed above, when $|K|$ increases, the pinning centers become more attractive for the skyrmion domain wall, shifting the depinning transition to a larger applied current density.

The shape of the skyrmion velocity-current curve shown in Fig. 5 is preserved only for $|K| \leq 0.04J$. In this regime, the velocity-current curve exhibits the three distinct dynamic phases discussed in the previous sections: (i) the pinned phase, (ii) soliton motion, and (iii) quasi-free skyrmion motion. In contrast, for $|K| > 0.04J$ the velocity exhibits a spike followed by a strong drop. The depinning transition, velocity spike, and velocity drop are shifted as the transport current density increases. In this regime, four dynamic phases are present: (i) the pinned phase, (ii) soliton motion, (iii) a reentrant pinned phase, and (iv) quasi-free skyrmion motion. Phases (i), (ii), and (iv) are the

same as those already described in the previous section, but the reentrant pinning phase is different. During the reentrant pinning phase, skyrmions are initially flowing following the previous soliton motion, but then the interstitial skyrmion, and in some cases more skyrmions depending on $|K|$, is annihilated inside the sample due to the stronger pinning produced by larger $|K|$. As a result of the annihilation, the soliton is destroyed and the remaining skyrmions become trapped at the pinning sites, leading to the emergence of a pinned state. Note that $\langle v_x \rangle \neq 0$ since the skyrmion is annihilated in this process, so that $\langle v_x \rangle \approx 0$ but we do not have $\langle v_x \rangle = 0$.

In Fig. 7(b) we plot the topological charge as a function of applied current density. For $K = -0.02J$ there is only a single transition in Q . The number of skyrmions is constant until $j = 4.4 \times 10^{10} \text{ A/m}^2$, above which all skyrmions are annihilated. For $K = -0.04J$, at $j = 2.9 \times 10^{10} \text{ A/m}^2$ seven skyrmions are annihilated, corresponding to the point between the soliton motion and the quasi-free motion shown in Fig. 7(a). It is important to note that for each value of j , the initial skyrmion configuration is the same as that illustrated in Fig. 1, meaning that the applied current is not swept up from zero. The goal is to simulate a sample with an interstitial skyrmion at different values of j to see how it behaves. When $K = -0.04J$, for $2.9 \times 10^{10} < j < 5 \times 10^{10} \text{ A/m}^2$ no additional annihilation is observed, while for $j > 5 \times 10^{10} \text{ A/m}^2$ all of the skyrmions annihilate. For $K = -0.06J$ there are two current densities at which two skyrmions are annihilated ($j = 2.9 \times 10^{10} \text{ A/m}^2$ and $j = 3.2 \times 10^{10} \text{ A/m}^2$). The annihilation of these two skyrmions terminates the soliton motion and causes $\langle v_x \rangle$ to drop to $\langle v_x \rangle \approx 0$. For $j = 3.5 \times 10^{10} \text{ A/m}^2$, 20 skyrmions are annihilated. This is the j value just before the quasi-free skyrmion motion, indicating that the reentrant pinning phase is a transient phase between the soliton and the quasi-free regime. For larger current density values $j \geq 5.3 \times 10^{10} \text{ A/m}^2$, all of the skyrmions are annihilated for $K = -0.06J$. At $K = -0.08J$, there is a region where few skyrmions are annihilated, annihilation of a single skyrmion for $j = 3.2 \times 10^{10} \text{ A/m}^2$, and annihilation of two skyrmions for $j = 3.5 \times 10^{10} \text{ A/m}^2$ and $3.8 \times 10^{10} \text{ A/m}^2$. The skyrmion annihilation destroys the soliton motion and generates the reentrant pinning phase. For $j \geq 5.6 \times 10^{10} \text{ A/m}^2$ all of the skyrmions in the sample are annihilated. The onset of complete skyrmion annihilation shifts to higher values of j with increasing $|K|$. When the interaction between skyrmions and pinning centers is stronger, the interstitial skyrmion requires more energy to push a pinned skyrmion from its pinning site. As a consequence, the interstitial skyrmion interacts with the rigid wall of the pinned skyrmion for a longer period of time, increasing the chances of annihilation.

6. Summary

Using an atomistic model for atomic magnetic moments, we simulated the dynamical behavior of a skyrmion chain in a nanotrack embedded with pinning centers and encased by rigid magnetic walls to guide the skyrmion motion along the x direction. The system is slightly off the commensuration ratio, resulting in the appearance of an interstitial skyrmion that creates a high mobility soliton in the lattice. As we apply a transport current density, the interstitial skyrmion pushes its neighboring pinned skyrmion into an interstitial position, and the previously interstitial skyrmion becomes pinned by the now vacant pinning site. This process occurs in a repeating sequence. The soliton motion is the result of a combination of interactions between the interstitial skyrmion, rigid walls, pinning centers, and pinned skyrmions.

We identified two peaks and a valley in the skyrmion velocity signal as a function of time. The first, weaker peak corresponds to the moment when a pinned skyrmion depins from the pinning center due to its interaction with the arriving interstitial skyrmion. The second, stronger peak

arises from a velocity boost due to the interaction of the skyrmion with a rigid wall. The valley represents the point at which the interstitial skyrmion slows down because it has begun to interact with the next pinned skyrmion in the chain. The soliton motion repeats indefinitely in a periodic manner, with the period controlled by the pinning density, illustrating the stability of the soliton motion. Using a velocity heat map plotted as a function of position and time, we observe that the soliton motion is linear in time with a constant velocity. This precise and controllable motion can be of value for technological applications where precise control of skyrmion motion is essential.

By varying the applied current density we obtain a range of j values for which the soliton motion is stable. For $K = -0.02J$, soliton motion exists over the range $1.2 \times 10^{10} \text{ A/m}^2 \leq j \leq 2.1 \times 10^{10} \text{ A/m}^2$, and is accompanied by a nonlinear velocity-current signature consistent with what was found in previous particle-based studies of soliton motion in skyrmion chains. We also show that the soliton moves much more rapidly than the individual skyrmions, and thus solitons have promise for use as fast and energy-efficient information carriers, since they can be set into motion using very low external current densities. For $j < 1.2 \times 10^{10} \text{ A/m}^2$ the system remains pinned since the external current density is too low to overcome the pinning force. When $j > 2.1 \times 10^{10} \text{ A/m}^2$, the soliton motion is destroyed and the velocity-current curve increases linearly with j since all the skyrmions have depinned and undergo quasi-free motion. In this regime, interactions with the pinning centers produce a velocity oscillation as a function of time with a frequency determined by the pinning density and applied current density. For $K = -0.02J$ there is no skyrmion annihilation until $j \geq 4.7 \times 10^{10} \text{ A/m}^2$, above which all of the skyrmions annihilate.

We also investigated the effects of the anisotropy strength K of the pinning sites. As $|K|$ increases, the onset of soliton motion shifts to higher values of j since larger applied current densities are required to depin skyrmions from stronger pinning centers. The velocity-current shape does not remain the same for all values of K . When $|K| \leq 0.04J$, soliton motion extends over a range of j values and the velocity-current curve is very similar in form to previous particle-based studies of soliton motion in skyrmion chains [73]. On the other hand, for $|K| \geq 0.06J$ the average skyrmion velocity behavior changes significantly and soliton motion occurs only over very restricted values of j . The change is a consequence of skyrmion annihilation, which destroys the soliton motion. The annihilation profile varies as a function of $|K|$, and the onset of complete skyrmion annihilation shifts to higher values of j with increasing $|K|$. The annihilation process produces a reentrant pinning phase, where skyrmions cease moving when the soliton is destroyed. The reentrant pinning phase falls between the soliton phase and the quasi-free skyrmion motion phase. Our results indicate that stable soliton motion in skyrmions is possible and can occur under conditions where the effects of the skyrmion Hall angle are strongly reduced. This could be useful for technological applications by providing precise and controllable information transmission via soliton motion.

Credit authorship contribution statement

J. C. Bellizotti Souza: Investigation, Software, Images, Writing - Original Draft **Nicolas Vizarim:** Methodology, Investigation, Images, Visualization, Writing - Review & Editing. **Charles Reichhardt:** Conceptualization, Methodology, Writing - Review & Editing. **Pablo Venegas:** Supervision, Funding acquisition. **Cynthia Reichhardt:** Software, Methodology, Writing - Review & Editing.

Declaration of Competing Interest

The authors declare that they have no known competing financial interests or personal relationships that could have appeared to influence the work reported in this paper.

Acknowledgment

This work was supported by the US Department of Energy through the Los Alamos National Laboratory. Los Alamos National Laboratory is operated by Triad National Security, LLC, for the National Nuclear Security Administration of the U. S. Department of Energy (Contract No. 892333218NCA000001).

J.C.B.S acknowledges funding from Fundação de Amparo à Pesquisa do Estado de São Paulo - FAPESP (Grant 2022/14053-8) and Coordenação de Aperfeiçoamento de Pessoal de Nível Superior - CAPES.

N.P.V acknowledges funding from Fundação de Amparo à Pesquisa do Estado de São Paulo - FAPESP (2017/20976-3).

References

- [1] S. Das Sarma, M. Freedman, C. Nayak, Topologically protected qubits from a possible non-Abelian fractional quantum Hall state, *Phys. Rev. Lett.* 94 (2005) 166802. [doi:10.1103/PhysRevLett.94.166802](https://doi.org/10.1103/PhysRevLett.94.166802).
- [2] J. E. Moore, The birth of topological insulators, *Nature* 464 (2010) 194–198. [doi:10.1038/nature08916](https://doi.org/10.1038/nature08916).
- [3] M. Z. Hasan, C. L. Kane, Colloquium: Topological insulators, *Rev. Mod. Phys.* 82 (2010) 3045–3067. [doi:10.1103/RevModPhys.82.3045](https://doi.org/10.1103/RevModPhys.82.3045).
- [4] S. Mühlbauer, B. Binz, F. Jonietz, C. Pfleiderer, A. Rosch, A. Neubauer, R. Georgii, P. Böni, Skyrmion lattice in a chiral magnet, *Science* 323 (5916) (2009) 915–919. [doi:10.1126/science.1166767](https://doi.org/10.1126/science.1166767).
- [5] X. Z. Yu, Y. Onose, N. Kanazawa, J. H. Park, J. H. Han, Y. Matsui, N. Nagaosa, Y. Tokura, Real-space observation of a two-dimensional skyrmion crystal, *Nature (London)* 465 (7300) (2010) 901–904. [doi:10.1038/nature09124](https://doi.org/10.1038/nature09124).
- [6] A. Fert, V. Cros, J. Sampaio, Skyrmions on the track, *Nature Nanotechnol.* 8 (3) (2013) 152–156. [doi:10.1038/nnano.2013.29](https://doi.org/10.1038/nnano.2013.29).
- [7] N. Nagaosa, Y. Tokura, Topological properties and dynamics of magnetic skyrmions, *Nature Nanotechnol.* 8 (12) (2013) 899–911. [doi:10.1038/NNANO.2013.243](https://doi.org/10.1038/NNANO.2013.243).
- [8] K. Litzius, I. Lemesh, B. Krüger, P. Bassirian, L. Caretta, K. Richter, F. Büttner, K. Sato, O. A. Tretiakov, J. Förster, R. M. Reeve, M. Weigand, I. Bykova, H. Stoll, G. Schütz, G. S. D. Beach, M. Kläui, Skyrmion Hall effect revealed by direct time-resolved X-ray microscopy, *Nature Phys.* 13 (2) (2017) 170–175. [doi:10.1038/NPHYS4000](https://doi.org/10.1038/NPHYS4000).
- [9] K. Everschor-Sitte, J. Masell, R. M. Reeve, M. Klaüi, Perspective: Magnetic skyrmions - Overview of recent progress in an active research field, *J. Appl. Phys.* 124 (24) (2018) 240901. [doi:10.1063/1.5048972](https://doi.org/10.1063/1.5048972).
- [10] A. Fert, N. Reyren, V. Cros, Magnetic skyrmions: advances in physics and potential applications, *Nature Rev. Mater.* 2 (7) (2017) 17031. [doi:10.1038/natrevmats.2017.31](https://doi.org/10.1038/natrevmats.2017.31).

- [11] S. Luo, M. Song, X. Li, Y. Zhang, J. Hong, X. Yang, X. Zou, N. Xu, L. You, Reconfigurable skyrmion logic gates, *Nano Lett.* 18 (2) (2018) 1180–1184. doi:10.1021/acs.nanolett.7b04722.
- [12] Y. Shu, Q. Li, J. Xia, P. Lai, Z. Hou, Y. Zhao, D. Zhang, Y. Zhou, X. Liu, G. Zhao, Realization of the skyrmionic logic gates and diodes in the same racetrack with enhanced and modified edges, *Appl. Phys. Lett.* 121 (2022) 042402. doi:10.1063/5.0097152.
- [13] X. Zhang, M. Ezawa, Y. Zhou, Magnetic skyrmion logic gates: conversion, duplication and merging of skyrmions, *Sci. Rep.* 5 (2015) 9400. doi:10.1038/srep09400.
- [14] X. Zhang, Y. Zhou, M. Ezawa, G. P. Zhao, W. Zhao, Magnetic skyrmion transistor: skyrmion motion in a voltage-gated nanotrack, *Sci. Rep.* 5 (2015) 11369. doi:10.1038/srep11369.
- [15] J. C. Bellizotti Souza, N. P. Vizarim, C. J. O. Reichhardt, C. Reichhardt, P. A. Venegas, Clogging, diode and collective effects of skyrmions in funnel geometries, *New J. Phys.* 24 (2022) 103030. doi:10.1088/1367-2630/ac9749.
- [16] J. C. Bellizotti Souza, N. P. Vizarim, C. J. O. Reichhardt, C. Reichhardt, P. A. Venegas, Magnus induced diode effect for skyrmions in channels with periodic potentials, *J. Phys.: Condens. Matter* 35 (2023) 015804. doi:10.1088/1361-648X/ac9cc5.
- [17] Y. Feng, X. Zhang, G. Zhao, G. Xiang, A skyrmion diode based on skyrmion Hall effect, *IEEE Trans. Electron Devices* 69 (2022) 1293. doi:10.1109/TED.2021.3138837.
- [18] J. Wang, J. Xia, X. Zhang, X. Zheng, G. Li, L. Chen, Y. Zhou, J. Wu, H. Yin, R. Chantrell, Y. Xu, Magnetic skyrmion diode with a magnetic anisotropy voltage gating, *Appl. Phys. Lett.* 117 (20) (2020) 202401. doi:10.1063/5.0025124.
- [19] L. Song, H. Yang, B. Liu, H. Meng, Y. Cao, P. Yan, A spin-wave driven skyrmion diode under transverse magnetic fields, *J. Mag. Mag. Mater.* 532 (2021) 167975. doi:10.1016/j.jmmm.2021.167975.
- [20] D.-H. Jung, H.-S. Han, N. Kim, G. Kim, S. Jeong, S. Lee, M. Kang, M.-Y. Im, K.-S. Lee, Magnetic skyrmion diode: Unidirectional skyrmion motion via symmetry breaking of potential energy barriers, *Phys. Rev. B* 104 (2021) L060408. doi:10.1103/PhysRevB.104.L060408.
- [21] L. Zhao, X. Liang, J. Xia, G. Zhao, Y. Zhou, A ferromagnetic skyrmion-based diode with a voltage-controlled potential barrier, *Nanoscale* 17 (2020) 9507. doi:10.1039/C9NR10528J.
- [22] C. Pfleiderer, Surfaces get hairy, *Nature Phys.* 7 (2011) 673–674. doi:10.1038/nphys2081.
- [23] R. Wiesendanger, Nanoscale magnetic skyrmions in metallic films and multilayers: a new twist for spintronics, *Nature Rev. Mater.* 1 (7) (2016) 16044. doi:10.1038/natrevmats.2016.44.
- [24] W. Kang, Y. Huang, X. Zhang, Y. Zhou, W. Zhao, Skyrmion-electronics: an overview and outlook, *Proc. IEEE* 104 (10) (2016) 2040–2061. doi:10.1109/JPROC.2016.2591578.
- [25] C. Reichhardt, C. J. O. Reichhardt, Depinning and nonequilibrium dynamic phases of particle assemblies driven over random and ordered substrates: a review, *Rep. Prog. Phys.* 80 (2) (2017) 026501. doi:10.1088/1361-6633/80/2/026501.

- [26] J. Iwasaki, M. Mochizuki, N. Nagaosa, Universal current-velocity relation of skyrmion motion in chiral magnets, *Nature Commun.* 4 (2013) 1463. doi:10.1038/ncomms2442.
- [27] W. Jiang, X. Zhang, G. Yu, W. Zhang, X. Wang, M. B. Jungfleisch, J. E. Pearson, X. Cheng, O. Heinonen, K. L. Wang, Y. Zhou, A. Hoffmann, S. G. E. te Velthuis, Direct observation of the skyrmion Hall effect, *Nature Phys.* 13 (2) (2017) 162–169. doi:10.1038/NPHYS3883.
- [28] S.-Z. Lin, C. Reichhardt, C. D. Batista, A. Saxena, Driven skyrmions and dynamical transitions in chiral magnets, *Phys. Rev. Lett.* 110 (2013) 207202. doi:10.1103/PhysRevLett.110.207202.
- [29] S.-Z. Lin, C. Reichhardt, C. D. Batista, A. Saxena, Particle model for skyrmions in metallic chiral magnets: Dynamics, pinning, and creep, *Phys. Rev. B* 87 (2013) 214419. doi:10.1103/PhysRevB.87.214419.
- [30] K. Zeissler, S. Finizio, C. Barton, A. J. Huxtable, J. Massey, J. Raabe, A. V. Sadovnikov, S. A. Nikitov, R. Brearton, T. Hesjedal, G. van der Laan, M. C. Rosamond, E. H. Linfield, G. Burnell, C. H. Marrows, Diameter-independent skyrmion Hall angle observed in chiral magnetic multilayers, *Nature Commun.* 11 (1) (2020) 428. doi:10.1038/s41467-019-14232-9.
- [31] X. Zhang, J. Xia, G. P. Zhao, X. Liu, Y. Zhou, Magnetic skyrmion transport in a nanotrack with spatially varying damping and non-adiabatic torque, *IEEE Trans. Magn.* 53 (3) (2017) 1500206. doi:10.1109/TMAG.2016.2641384.
- [32] R. Brearton, L. A. Turnbull, J. A. T. Verezhak, G. Balakrishnan, P. D. Hatton, G. van der Laan, T. Hesjedal, Deriving the skyrmion Hall angle from skyrmion lattice dynamics, *Nature Commun.* 12 (2021) 2723. doi:10.1038/s41467-021-22857-y.
- [33] C. Reichhardt, D. Ray, C. J. O. Reichhardt, Quantized transport for a skyrmion moving on a two-dimensional periodic substrate, *Phys. Rev. B* 91 (2015) 104426. doi:10.1103/PhysRevB.91.104426.
- [34] C. Reichhardt, D. Ray, C. J. O. Reichhardt, Nonequilibrium phases and segregation for skyrmions on periodic pinning arrays, *Phys. Rev. B* 98 (2018) 134418. doi:10.1103/PhysRevB.98.134418.
- [35] J. Feilhauer, S. Saha, J. Tobik, M. Zelent, L. J. Heyderman, M. Mruczkiewicz, Controlled motion of skyrmions in a magnetic antidot lattice, *Phys. Rev. B* 102 (2020) 184425. doi:10.1103/PhysRevB.102.184425.
- [36] N. P. Vizarim, J. C. Bellizotti Souza, C. Reichhardt, C. J. O. Reichhardt, P. A. Venegas, Directional locking and the influence of obstacle density on skyrmion dynamics in triangular and honeycomb arrays, *J. Phys.: Condens. Matter* 33 (2021) 305801. doi:10.1088/1361-648X/ac0081.
- [37] N. P. Vizarim, C. Reichhardt, P. A. Venegas, C. J. O. Reichhardt, Shapiro steps and nonlinear skyrmion Hall angles for dc and ac driven skyrmions on a two-dimensional periodic substrate, *Phys. Rev. B* 102 (2020) 104413. doi:10.1103/PhysRevB.102.104413.

[38] N. P. Vizarim, C. Reichhardt, C. J. O. Reichhardt, P. A. Venegas, Skyrmiion dynamics and topological sorting on periodic obstacle arrays, *New J. Phys.* 22 (2020) 053025. doi:10.1088/1367-2630/ab8045.

[39] N. P. Vizarim, C. J. O. Reichhardt, P. A. Venegas, C. Reichhardt, Skyrmiion dynamics and transverse mobility: skyrmiion Hall angle reversal on 2D periodic substrates with dc and bi-harmonic ac drives, *Eur. Phys. J. B* 93 (2020) 112. doi:10.1140/epjb/e2020-10135-1.

[40] N. P. Vizarim, C. J. O. Reichhardt, P. A. Venegas, C. Reichhardt, Skyrmiion pinball and directed motion on obstacle arrays, *J. Phys. Commun.* 4 (2020) 085001. doi:10.1088/2399-6528/aba9fb.

[41] C. J. O. Reichhardt, C. Reichhardt, Commensurability, jamming, and dynamics for vortices in funnel geometries, *Phys. Rev. B* 81 (2010) 224516. doi:10.1103/PhysRevB.81.224516.

[42] C. Reichhardt, D. Ray, C. J. O. Reichhardt, Magnus-induced ratchet effects for skyrmions interacting with asymmetric substrates, *New J. Phys.* 17 (2015) 073034. doi:10.1088/1367-2630/17/7/073034.

[43] B. Göbel, I. Mertig, Skyrmiion ratchet propagation: utilizing the skyrmiion Hall effect in AC racetrack storage devices, *Sci. Rep.* 11 (2021) 3020. doi:10.1038/s41598-021-81992-0.

[44] J. C. B. Souza, N. P. Vizarim, C. J. O. Reichhardt, C. Reichhardt, P. A. Venegas, Skyrmiion ratchet in funnel geometries, *Phys. Rev. B* 104 (2021) 054434. doi:10.1103/PhysRevB.104.054434.

[45] W. Chen, L. Liu, Y. Ji, Y. Zheng, Skyrmiion ratchet effect driven by a biharmonic force, *Phys. Rev. B* 99 (2019) 064431. doi:10.1103/PhysRevB.99.064431.

[46] N. P. Vizarim, C. Reichhardt, P. A. Venegas, C. J. O. Reichhardt, Guided skyrmiion motion along pinning array interfaces, *J. Mag. Mag. Mater.* 528 (2021) 167710. doi:<https://doi.org/10.1016/j.jmmm.2020.167710>.

[47] C.-L. Zhang, J.-N. Wang, C.-K. Song, N. Mehmood, Z.-Z. Zeng, Y.-X. Ma, J.-B. Wang, Q.-F. Liu, Edge-guided heart-shaped skyrmiion, *Rare Metals* 41 (2022) 865–870. doi:10.1007/s12598-021-01844-8.

[48] R. Yanes, F. Garcia-Sanchez, R. F. Luis, E. Martinez, V. Raposo, L. Torres, L. Lopez-Diaz, Skyrmiion motion induced by voltage-controlled in-plane strain gradients, *Appl. Phys. Lett.* 115 (2019) 132401. doi:10.1063/1.5119085.

[49] S. L. Zhang, W. W. Wang, D. M. Burn, H. Peng, H. Berger, A. Bauer, C. Pfleiderer, G. van der Laan, T. Hesjedal, Manipulation of skyrmiion motion by magnetic field gradients, *Nature Commun.* 9 (2018) 2115. doi:10.1038/s41467-018-04563-4.

[50] K. Everschor, M. Garst, B. Binz, F. Jonietz, S. Mühlbauer, C. Pfleiderer, A. Rosch, Rotating skyrmiion lattices by spin torques and field or temperature gradients, *Phys. Rev. B* 86 (2012) 054432. doi:10.1103/PhysRevB.86.054432.

[51] L. Kong, J. Zang, Dynamics of an insulating skyrmiion under a temperature gradient, *Phys. Rev. Lett.* 111 (2013) 067203. doi:10.1103/PhysRevLett.111.067203.

[52] V. L. Carvalho-Santos, M. A. Castro, D. Salazar-Aravena, D. Laroze, R. M. Corona, S. Allende, D. Altbir, Skyrmion propagation along curved racetracks, *Appl. Phys. Lett.* 118 (2021) 172407. [doi:10.1063/5.0045969](https://doi.org/10.1063/5.0045969).

[53] A. Korniienko, A. Kákay, D. D. Sheka, V. P. Kravchuk, Effect of curvature on the eigenstates of magnetic skyrmions, *Phys. Rev. B* 102 (2020) 014432. [doi:10.1103/PhysRevB.102.014432](https://doi.org/10.1103/PhysRevB.102.014432).

[54] K. V. Yershov, A. Kákay, V. P. Kravchuk, Curvature-induced drift and deformation of magnetic skyrmions: Comparison of the ferromagnetic and antiferromagnetic cases, *Phys. Rev. B* 105 (2022) 054425. [doi:10.1103/PhysRevB.105.054425](https://doi.org/10.1103/PhysRevB.105.054425).

[55] R. M. Menezes, J. F. S. Neto, C. C. d. S. Silva, M. V. Milošević, Manipulation of magnetic skyrmions by superconducting vortices in ferromagnet-superconductor heterostructures, *Phys. Rev. B* 100 (2019) 014431. [doi:10.1103/PhysRevB.100.014431](https://doi.org/10.1103/PhysRevB.100.014431).

[56] X. Zhang, J. Xia, X. Liu, Structural transition of skyrmion quasiparticles under compression, *Phys. Rev. B* 105 (2022) 184402. [doi:10.1103/PhysRevB.105.184402](https://doi.org/10.1103/PhysRevB.105.184402).

[57] J. C. Bellizotti Souza, N. P. Vizirim, C. J. O. Reichhardt, C. Reichhardt, P. A. Venegas, Spontaneous skyrmion conformal lattice and transverse motion during dc and ac compression, *New J. Phys.* 25 (2023) 053020. [doi:10.1088/1367-2630/acd46f](https://doi.org/10.1088/1367-2630/acd46f).

[58] X. Zhang, J. Xia, O. A. Tretiakov, M. Ezawa, G. Zhao, Y. Zhou, X. Li, M. Mochizuki, Laminar and quasi-turbulent dynamics of a magnetic skyrmion pipe flow (2023). [arXiv:arXiv:2305.13590](https://arxiv.org/abs/2305.13590).

[59] U. Welp, Z. L. Xiao, V. Novosad, V. K. Vlasko-Vlasov, Commensurability and strong vortex pinning in nanopatterned Nb films, *Phys. Rev. B* 71 (2005) 014505. [doi:10.1103/PhysRevB.71.014505](https://doi.org/10.1103/PhysRevB.71.014505).

[60] C. Reichhardt, C. J. Olson, F. Nori, Nonequilibrium dynamic phases and plastic flow of driven vortex lattices in superconductors with periodic arrays of pinning sites, *Phys. Rev. B* 58 (1998) 6534–6564. [doi:10.1103/PhysRevB.58.6534](https://doi.org/10.1103/PhysRevB.58.6534).

[61] K. Harada, O. Kamimura, H. Kasai, T. Matsuda, A. Tonomura, V. V. Moshchalkov, Direct observation of vortex dynamics in superconducting films with regular arrays of defects, *Science* 274 (5290) (1996) 1167–1170. [doi:10.1126/science.274.5290.1167](https://doi.org/10.1126/science.274.5290.1167).

[62] K. Mangold, P. Leiderer, C. Bechinger, Phase transitions of colloidal monolayers in periodic pinning arrays, *Phys. Rev. Lett.* 90 (2003) 158302. [doi:10.1103/PhysRevLett.90.158302](https://doi.org/10.1103/PhysRevLett.90.158302).

[63] D. G. Rees, H. Totsuji, K. Kono, Commensurability-dependent transport of a Wigner crystal in a nanoconstriction, *Phys. Rev. Lett.* 108 (2012) 176801. [doi:10.1103/PhysRevLett.108.176801](https://doi.org/10.1103/PhysRevLett.108.176801).

[64] H. Pu, L. O. Baksmaty, S. Yi, N. P. Bigelow, Structural phase transitions of vortex matter in an optical lattice, *Phys. Rev. Lett.* 94 (2005) 190401. [doi:10.1103/PhysRevLett.94.190401](https://doi.org/10.1103/PhysRevLett.94.190401).

[65] S. Tung, V. Schweikhard, E. A. Cornell, Observation of vortex pinning in Bose-Einstein condensates, *Phys. Rev. Lett.* 97 (2006) 240402. [doi:10.1103/PhysRevLett.97.240402](https://doi.org/10.1103/PhysRevLett.97.240402).

[66] C. J. Olson Reichhardt, S. Z. Lin, D. Ray, C. Reichhardt, Comparing the dynamics of skyrmions and superconducting vortices, *Physica C* 503 (2014) 52. [doi:10.1016/j.physc.2014.03.029](https://doi.org/10.1016/j.physc.2014.03.029).

[67] C. Reichhardt, C. J. O. Reichhardt, Commensuration effects on skyrmion Hall angle and drag for manipulation of skyrmions on two-dimensional periodic substrates, *Phys. Rev. B* 105 (2022) 214437. [doi:10.1103/PhysRevB.105.214437](https://doi.org/10.1103/PhysRevB.105.214437).

[68] J. Gutierrez, A. V. Silhanek, J. Van de Vondel, W. Gillijns, V. V. Moshchalkov, Transition from turbulent to nearly laminar vortex flow in superconductors with periodic pinning, *Phys. Rev. B* 80 (2009) 140514. [doi:10.1103/PhysRevB.80.140514](https://doi.org/10.1103/PhysRevB.80.140514).

[69] T. Bohlein, J. Mikhael, C. Bechinger, Observation of kinks and antikinks in colloidal monolayers driven across ordered surfaces, *Nature Mater.* 11 (2) (2012) 126–130. [doi:10.1038/NMAT3204](https://doi.org/10.1038/NMAT3204).

[70] A. Vanossi, N. Manini, E. Tosatti, Static and dynamic friction in sliding colloidal monolayers, *Proc. Natl. Acad. Sci. (USA)* 109 (41) (2012) 16429–16433. [doi:10.1073/pnas.1213930109](https://doi.org/10.1073/pnas.1213930109).

[71] M. P. N. Juniper, A. V. Straube, R. Besseling, D. G. A. L. Aarts, R. P. A. Dullens, Microscopic dynamics of synchronization in driven colloids, *Nature Commun.* 6 (2015) 7187. [doi:10.1038/ncomms8187](https://doi.org/10.1038/ncomms8187).

[72] A. Benassi, A. Vanossi, E. Tosatti, Nanofriction in cold ion traps, *Nature Commun.* 2 (2011) 236. [doi:10.1038/ncomms1230](https://doi.org/10.1038/ncomms1230).

[73] N. P. Vizarim, J. C. B. Souza, C. J. O. Reichhardt, C. Reichhardt, M. V. Milošević, P. A. Venegas, Soliton motion in skyrmion chains: Stabilization and guidance by nanoengineered pinning, *Phys. Rev. B* 105 (2022) 224409. [doi:10.1103/PhysRevB.105.224409](https://doi.org/10.1103/PhysRevB.105.224409).

[74] R. F. L. Evans, Atomistic Spin Dynamics, in: W. Andreoni, S. Yip (Eds.), *Handbook of Materials Modeling: Applications: Current and Emerging Materials*, Springer International Publishing, 2018, pp. 1–23. [doi:10.1007/978-3-319-50257-1_147-1](https://doi.org/10.1007/978-3-319-50257-1_147-1).

[75] J. Iwasaki, M. Mochizuki, N. Nagaosa, Current-induced skyrmion dynamics in constricted geometries, *Nature Nanotechnol.* 8 (10) (2013) 742–747. [doi:10.1038/nnano.2013.176](https://doi.org/10.1038/nnano.2013.176).

[76] S. Seki, M. Mochizuki, *Skyrmions in Magnetic Materials*, Springer International Publishing, 2016, series Title: SpringerBriefs in Physics. [doi:10.1007/978-3-319-24651-2](https://doi.org/10.1007/978-3-319-24651-2).

[77] D. Stosic, T. B. Ludermir, M. V. Milošević, Pinning of magnetic skyrmions in a monolayer Co film on Pt(111): Theoretical characterization and exemplified utilization, *Physical Review B* 96 (21) (2017) 214403. [doi:10.1103/PhysRevB.96.214403](https://doi.org/10.1103/PhysRevB.96.214403).

[78] J. C. Slonczewski, Dynamics of magnetic domain walls, *AIP Conference Proceedings* 5 (1) (1972) 170–174. [doi:10.1063/1.3699416](https://doi.org/10.1063/1.3699416).

[79] T. Gilbert, A phenomenological theory of damping in ferromagnetic materials, *IEEE Transactions on Magnetics* 40 (6) (2004) 3443–3449. [doi:10.1109/TMAG.2004.836740](https://doi.org/10.1109/TMAG.2004.836740).

[80] J. Zang, M. Mostovoy, J. H. Han, N. Nagaosa, Dynamics of Skyrmion Crystals in Metallic Thin Films, *Physical Review Letters* 107 (13) (2011) 136804. [doi:10.1103/PhysRevLett.107.136804](https://doi.org/10.1103/PhysRevLett.107.136804).

- [81] J.-V. Kim, J. Mulkers, On quantifying the topological charge in micromagnetics using a lattice-based approach, *IOP SciNotes* 1 (2) (2020) 25211. [doi:10.1088/2633-1357/abad0c](https://doi.org/10.1088/2633-1357/abad0c).
- [82] T. Schulz, R. Ritz, A. Bauer, M. Halder, M. Wagner, C. Franz, C. Pfleiderer, K. Everschor, M. Garst, A. Rosch, Emergent electrodynamics of skyrmions in a chiral magnet, *Nature Physics* 8 (4) (2012) 301–304. [doi:10.1038/nphys2231](https://doi.org/10.1038/nphys2231).